**ANAS Transactions** **Earth Sciences** **2 / 2024**

http://www.journalesgia.com

# PETROGENETIC ROLE OF PYROXENES IN THE FORMATION OF PICRITES OF THE LESSER CAUCASUS AND TALYSH ZONE

**Mammadov M.N., Babayeva G.J., Sariyev F.H.**

*Ministry of Science and Education of the Republic of Azerbaijan,*
*Institute of Geology and Geophysics, Azerbaijan*
*119, H.Javid ave., Baku, AZ1143: gultekin_babayeva@rambler.ru*

***Keywords:*** *The Lesser Caucasus, Talysh zone, picrite, zoned pyroxene, crystallization differentiation*

***Summary.*** On the basis of microprobe, chemical and X-ray diffractometric analyses, the petrogenetic features of the formation of picrites depending on epycompositional variability of clinopyroxenes in the Lesser Caucasus and Talysh zone were studied. The Upper Jurassic picrites of the Murovdag anticlinorium were formed under similar geological and geodynamic conditions, while being controlled by the rift-type crack structure. Therefore, the petrographic type of rocks involved in the anticlinorium is homogeneous. Clinopyroxene megacrysts in subalkaline picrites in the Khojavend bend correspond to chromium diopside partially depleted in titanium oxide. Clinopyroxenes are included as phenocrysts, normal prismatic and megacrysts in the Santonian trachybasalt-trachydolerite, tephrite-teschenite complexes of the Khojavend synclinorium. The contact zone is noticeable in its parent rock. In the Talysh zone, the picrites belong to the subalkaline series and have a characteristic clay structure, and their main masses are dolerite and subdolerite. Along with olivine, clinopyroxene phenocrysts are present in the contents. Those phenocrysts in most cases form large elongated, sometimes plate-like crystals. In most cases, they are colorless. However, olivine and chromspinel inclusions of different sizes are observed in them. Rather large prismatic phenocrysts of clinopyroxenes are included in phlogopite and olivine picrites. These phenocrysts are xenomorphic to olivine. The composition of clinopyroxenes in the picrites of Talysh zone corresponds to diopside-salite. Thus, the change in the composition of pieroxenes in picrites of the Lesser Caucasus and Talysh zone is regulated by crystallization differentiation.



**Introduction.** The formation of picrites is related to the melting of the mantle substrate at high degree. Therefore, their geochemical composition corresponds mainly to the composition of the core mantle. Besides these, in most cases, picrites are homogeneous both in oceans and continents of the world. In some cases, they are formed by the direct control of crystallization differentiation. In this sense, the study of the genesis of picrites is of great importance.

According to the existing geological and petrological sources, the study of monoclinic and rhombic pyroxenes, which are part of picrites, is the most realistic source of genetic information in determining the evolutionary processes of their primary fusion, thermobaric conditions of their crystallization, as well as their potential mineralization.

Unlike other rock-forming minerals, pyroxenes are more resistant to derivative processes and can preserve their originality. In this sense, the study of their complex physico-chemical and petrological characteristics can be quite important in the research of the petrological and geological conditions of picrites occurrences of the Lesser Caucasus and Talysh zone.

**Research methods.** Microprobe, chemical and X-ray diffraction methods were used to determine the reliability of the presented pyroxene analyses. Microprobe analyses of pyroxene phenocrysts were carried out using an internal standard in electron probe microanalysis (JEOL, JSM-6610 LV, Oxford Instruments, X-MAX). All microprobe, X-ray diffraction and chemical analyses of pyroxenes were carried out at the analytical center of the Institute of Geology and Geophysics of the Ministry of Science and Education of the Republic of Azerbaijan. The crystallochemical formulas of the minerals were determined by the Kushiro method (Kushiro, 1965), and the crystallization temperature was determined by the Lindsley paleothermometer (Lindsley, 1983).

**Geological and petrological conditions of the formation of picrites in the Lesser Caucasus and Talysh zone.** Picrites of various petrochemical series have been discovered in the geological structure of the Murovdag uplift, Khojavand flexure of the Lesser Caucasus and Talysh zone in the territory of the Republic of Azerbaijan.

Normal alkaline impregnation-like picrites are located in the Bajocian-Bathonian volcanites on the northeastern slope of the Murovdag uplift, at its junction with the Dashkasan flexure (Fig. 1).

Picrites are dark black and macroscopically homogeneous. But greenish-gray colored olivine phenocrysts are visible to the naked eye. A weak thermal rim is observed with volcanites of the contact zone. Picrites have characteristic porphyritic structure under the microscope. Olivine completely dominates among the phenocrysts (25-30%). They form large dipyramidal grains. Serpentine loops divided the olivine into separate parts. Olivine remained completely unaltered among the loops. The composition of the olivine phenocryst corresponds to forsterite-chrysolite ($Fa_{8-14\%}$), and in most cases it forms mutual combinations with chrome spinel. They are partially xenomorphic compared to rhombic and monoclinic olivine, and have spread very partially. Picrites are intensively chloritized in contact zones. They are low-graded in silica from a petrochemical point of view, and are accumulated in the area of typical picrites in the classification chart (Table 1, Fig. 2). It is clearly observed in the abovementioned classification chart that their points are accumulated together revealing the limitation of the weak evolutionary process. However, the weak increase of sericitization and calcitization in pyroxene picrites caused a partial increase of diopside in their normative mineralogical composition.

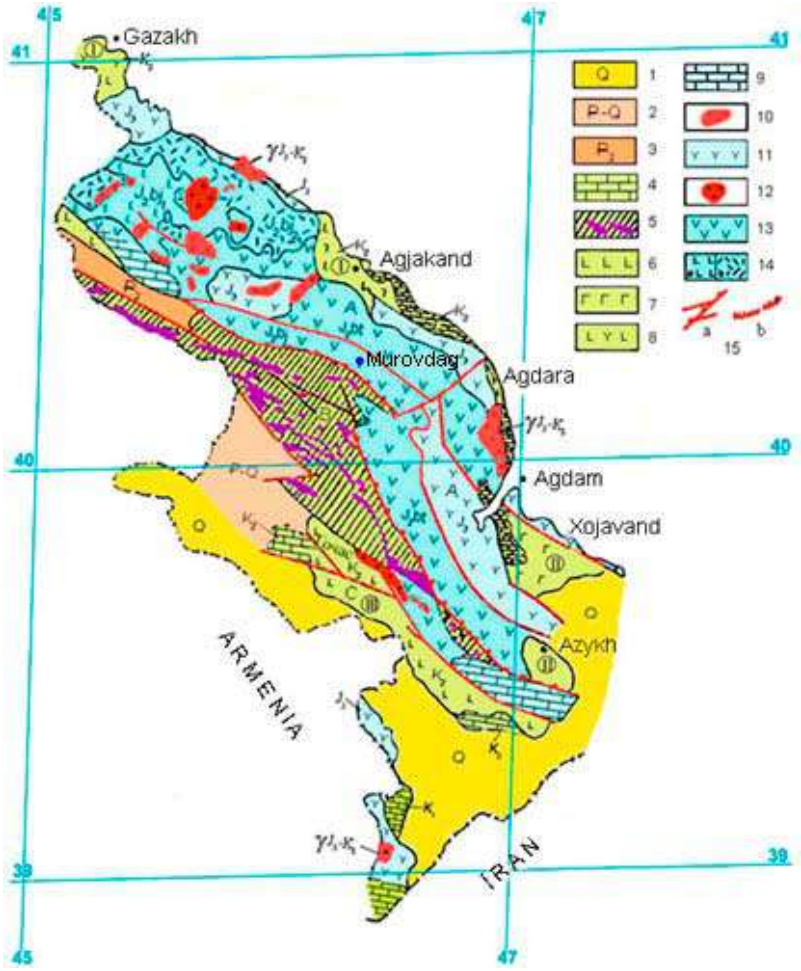


**Fig. 1.** Schematic geological map of the Lesser Caucasus (Шихалибейли, 1994)

I – Lok-Garabakh structural-formation zone (the Gazakh, the Agjakand, the Agdara depressions); II – Goycha-Akeri structural-formation zone (the Azykh and the Khojavand depressions), III – Miskhan-Kafan structural-formation zone (the Gochas depression) 1 – the contemporary sediments; 2 – the Paleogene-Neogene volcanogenic sedimentary deposits; 3 – the Paleogene volcanogenic sedimentary deposits; 4 – the Upper Cretaceous limestones; 5 –the ophiolite complexes; 6 – the Late Senonian basalt-andesibasalt and trachybasalt-trachyandesibasalt complexes (the Gochas depression); 7 – the Santonian basalt-andesibasalt and trachybasalt-trachyandesibasalt complexes (the Azykh depression), trachybasalt-trachydolerite and tephrite-teschenite (the Khojavand depression) complexes; 8 – the Late Coniacian-Early Santonian basalt-andesibasalt and the Late Santonian-Early Campanian rhyolite-rhyodacite complexes (the Gazakh depression), Coniacian-Santonian basalt-andesibasalt and rhyolite-rhyodacite complexes (the Agjakand and the Agdara depressions); 9 – the Upper Jurassic limestones; 10 – the Late Jura- Early Cretaceous gabbro-diorite-granite complex; 11 – the Late Jurassic- Early Cretaceous dacite complex; 12 – the Bathonian plagiogranite complex; 13 – the Bathonian basalt-andesite-dacite-rhyoilte complex; 14 – a) the Early Bajocian basalt complex, б) the Late Bajocian rhyolite complex; 15 – deep faults (a), flexures (b).

***Table 1***

Chemical and CIPW compositions of picrites of the Murovdag anticlinorium

| №№ / Komp. | 3 | 5 | 10 | 72 | 73 | 74 | 76 | 79 |
|---|---|---|---|---|---|---|---|---|
| $SiO_2$ | 41.45 | 42.50 | 41.60 | 41.21 | 42.28 | 42.15 | 43.36 | 43.60 |
| $TiO_2$ | 0.16 | 0.26 | 0.24 | 0.11 | 0.11 | 0.15 | 0.18 | 0.16 |
| $Al_2O_3$ | 7.12 | 6.70 | 6.23 | 9.56 | 7.46 | 9.12 | 9.11 | 8.78 |
| $Cr_2O_3$ | 0.38 | 0.34 | 0.24 | 0.46 | 0.38 | 0.42 | 0.58 | 0.46 |
| $Fe_2O_3$ | 3.42 | 4.56 | 3.64 | 3.92 | 3.75 | 3.89 | 3.42 | 3.95 |
| FeO | 5.53 | 6.14 | 6.04 | 6.49 | 6.79 | 6.40 | 5.60 | 6.51 |
| MnO | 0.18 | 0.19 | 0.22 | 0.17 | 0.18 | 0.16 | 0.20 | 0.16 |
| MgO | 31.78 | 28.80 | 28.81 | 28.85 | 29.36 | 27.42 | 25.20 | 25.70 |
| CaO | 5.53 | 5.66 | 8.26 | 4.23 | 5.28 | 6.20 | 7.30 | 6.40 |
| $Na_2O$ | 0.18 | 0.11 | 0.10 | 0.06 | 0.07 | 0.09 | 0.10 | 0.12 |
| $K_2O$ | 0.05 | 0.14 | 0.15 | 0.09 | 0.08 | 0.08 | 0.08 | 0.04 |
| $P_2O_5$ | 0.04 | 0.05 | 0.04 | 0.06 | 0.04 | 0.05 | 0.03 | 0.04 |
| LOI | 4.15 | 4.46 | 4.39 | 4.43 | 4.12 | 3.64 | 4.25 | 3.75 |
| ∑ | 99.97 | 99.91 | 99.96 | 99.64 | 99.90 | 99.77 | 99.41 | 99.67 |
| Ap | 0.1 | 0.1 | 0.1 | 0.1 | 0.1 | 0.1 | 0.1 | 0.1 |
| Il | 0.3 | 0.5 | 0.5 | 0.2 | 0.2 | 0.3 | 0.3 | 0.3 |
| Mt | 5.5 | 7.1 | 5.6 | 6.4 | 6.0 | 6.3 | 5.8 | 6.4 |
| Or | 0.3 | 0.8 | 0.9 | 0.5 | 0.5 | 0.5 | 0.5 | 0.2 |
| Ab | 1.5 | 0.9 | 0.8 | 0.5 | 0.6 | 0.8 | 0.8 | 1.0 |
| An | 18.5 | 17.4 | 16.1 | 20.6 | 19.8 | 24.2 | 24.2 | 23.3 |
| Di | 3.6 | 4.3 | 10.3 | - | 2.6 | 2.6 | 5.0 | 3.4 |
| En | 2.9 | 3.5 | 8.2 | - | 2.0 | 2.1 | 3.9 | 2.7 |
| Fs | 0.3 | 0.3 | 0.9 | - | 0.3 | 0.2 | 0.4 | 0.4 |
| Fo | 44.4 | 31.8 | 39.7 | 32.8 | 34.8 | 32.4 | 24.4 | 23.9 |
| Fa | 4.4 | 3.5 | 4.8 | 4.2 | 4.8 | 4.3 | 3.0 | 3.4 |
| En | 12.9 | 22.8 | 6.9 | 25.1 | 21.5 | 20.0 | 24.0 | 27.3 |
| Fs | 1.1 | 2.3 | 0.8 | 2.9 | 2.7 | 2.4 | 2.7 | 3.5 |
| ∑ | 95.8 | 95.3 | 95.6 | 93.3 | 95.9 | 96.2 | 95.1 | 95.9 |

3, 73 – olivine picrite, 5, 10, 72 ,74, 76, 79 – olivine-pyroxene picrite.

The results of the conducted petrochemical, petrographic and mineralogical studies show that indeed the picrite magma was poorly evolved in the Earth's crust.

The subalkaline analogs of picrites occur in association with tephrites, trachybasalts, and teshenites of the Khojavend Synclinorium of the Lesser Caucasian Megaanticlinorium. The described subalkaline picrites form a gradual transition with teschenite on the one hand, and tephrite on the other hand.

At the same time, a limited amount of chrome diopside and phlogopite inclusions of 0.5x5 cm size were found in the breccias of tephrite. A thin thermal contact is observed between those inclusions and tephrite. Teschenite is freckled-gray, dark-gray and gray-black colored and varies from top to bottom by gravity of rock types. Volcanites are located in the center of the Khojavand synclinorium surrounded by Santonian limestones.

Macroscopically, the picrites of the Khojavand synclinorium is dark black, and relatively greenish-black pyroxene grains, sometimes colorless and pale brown phlogopite grains are easily visible to the naked eye against their background.

Picrites of the Khojavand synclinorium is located in the contact zones of picrites and basalts in the classification chart (Table 2, Fig. 2) from the petrochemical point of view. The abundance of alkaline ($Na_2O+K_2O$), chrome and titanium oxides in contrast to the previous petrographic types of rocks shows some peculiarities of the primary fusion of these picrites. Besides these, the amount of magnesium oxide gradually decreases from 22.4% to 11.78%, starting from the subalkaline melanocrate type towards the leucocrate type due to other petrochemical characteristics of the subalkaline picrites. Such an alteration is also occurred in the normative mineralogical composition of picrites. So, the normative forsterite molecule decreases from olivine subalkaline picrites to leucocratic picrites (Table 2). The subalkaline picrites of the Khojavand synclinorium are nepheline normative.

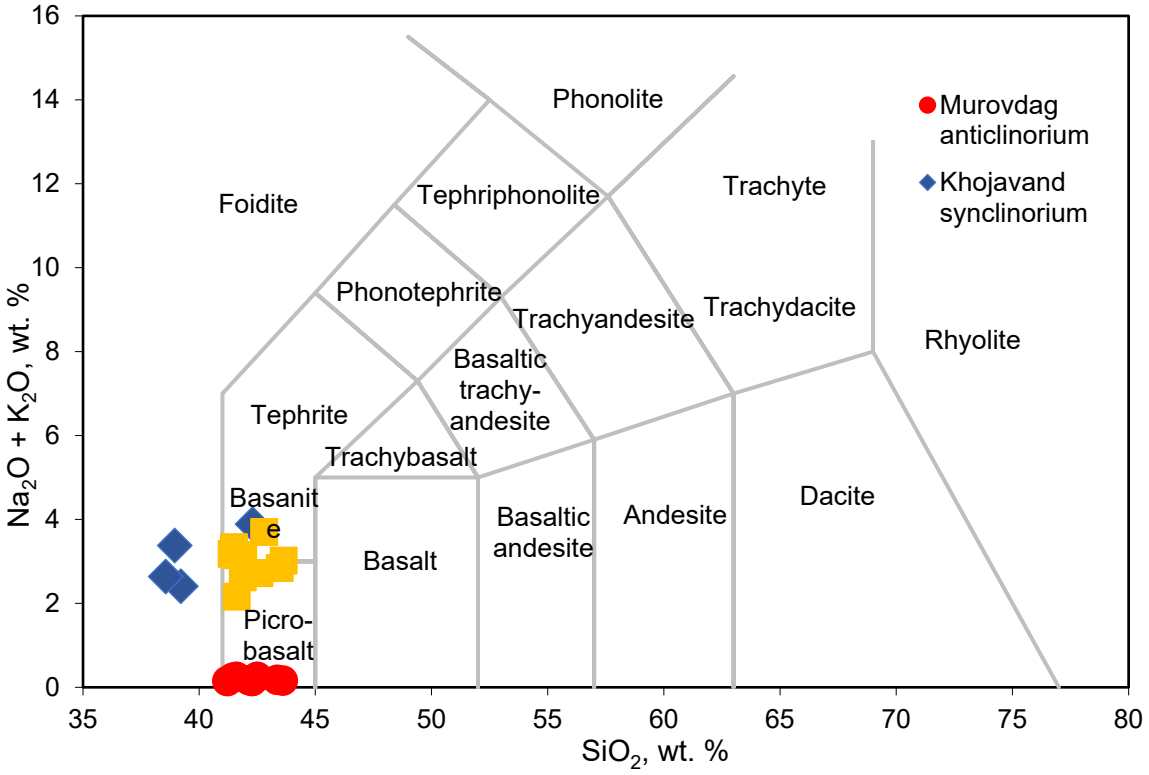


**Fig. 2.** Position of the chemical compositions of picrites of the Lesser Caucasus and Talysh zone on the TAS classification chart (Le Bas et al., 1986).

The Talysh zone is the northwestern continuation of the Alborz folding zone, it is traced from the valley of the Seyfirud (Agchay) River in the direction of the general Caucasus to the Germi settlement of the Islamic Republic of Iran (Fig. 3) (Азизбеков и др., 1979). The structures of the zone change the stretching direction from here and are observed along the latitudinal circle to the Garadag ophiolite outcrop (Мамедов, 1983; Рустамов, 2019). The picrites are of the subalkaline composition here and their age is mainly the Upper Eocene-Lower Oligocene. The subalkaline picrites form thin (2-4 m) layered outcrops alternating with the Paleocene and Eocene flysch sandstones in this zone. Besides these, picrite's limited outcrops of low thickness (2.5-3 m) are observed in places where picrites spread. But the subalkaline picrites are impregnated and fully crystalline. The large impregnations consist of monoclinic pyroxene of 0.3x1.2 cm size, olivine with relatively minor chrysotile, as well as phlogopite and small chrome spinel grains. The main mass of the rock is fully crystalline and consists of clinopyroxene grains. The subalkaline picrites are involved in serpentinization and amphibolization processes to one degree or another. The chemical and normative mineralogical composition of picrites is given in Table 3.

The amount of olivine, chrome diopside and chrome spinel in the composition of the subalkaline picrites gradually changes along the vertical section here too. Therefore, their plagioclase types are directly observed in the apical parts of picrites.

As abovementioned, the picrites found in the Lesser Caucasus and Talysh zones differ greatly in terms of their composition and occurrence conditions. Besides the geological and petrological properties of their formation, this diversity occurs in the compositional alteration of the rock-forming minerals involved in the composition of picrites, in the crystallization sequences and determination of thermal conditions. In this sense, the study of pyroxenes in the compositions of picrites of different ages and petrochemical series, which are distributed in the Lesser Caucasus and the Talysh zone, is of exceptional petrogenetic importance. So, the petrological and geological diversity of picrites developed in the abovementioned zones can be shown in the examples of pyroxenes that are part of their composition.

From this point of view, as abovementioned, the picrites found on the north-eastern slope of the Murovdag anticlinorium are less evolved and the monoclinic and rhombic pyroxenes in their compositions are almost homogeneous. According to the conducted microscopic research, rhombic and monoclinic pyroxenes are xenomorphic with a very small amount of impregnations compared to the olivine impregnations in the composition of picrites. Its impregnations are found in a short prismatic form (Fig. 4).

***Table 2***

Chemical and CIPW compositions of the subalkaline picrites of the Khojavend synclinorium

| an. / Komp. | 1 | 2 | 3 | 4 |
|---|---|---|---|---|
| $SiO_2$ | 39.21 | 38.56 | 38.95 | 42.3 |
| $TiO_2$ | 2.18 | 2.19 | 2.25 | 1.38 |
| $Al_2O_3$ | 8.46 | 8.86 | 11.12 | 14.29 |
| $Cr_2O_3$ | 1.48 | 1.49 | 0.84 | 0.64 |
| $Fe_2O_3$ | 3.76 | 3.64 | 3.46 | 3.57 |
| FeO | 6.45 | 6.75 | 6.73 | 7.28 |
| MnO | 0.18 | 0.2 | 0.23 | 0.18 |
| MgO | 22.4 | 21.5 | 17.4 | 11.78 |
| CaO | 8.16 | 7.64 | 9.6 | 9.82 |
| $Na_2O$ | 1.16 | 1.46 | 1.82 | 2.79 |
| $K_2O$ | 1.25 | 1.18 | 1.56 | 1.1 |
| $P_2O_5$ | 0.21 | 0.18 | 0.16 | 0.25 |
| LOI | 4.56 | 5.75 | 5.32 | 4.43 |
| ∑ | 99.46 | 99.4 | 99.44 | 99.81 |
| Ap | 0.1 | 0.1 | 0.1 | 0.7 |
| Il | 4.1 | 4.1 | 4.2 | 2.6 |
| Mgt | 7.4* | 7.5* | 6.5* | 5.6 |
| Or | 7.2 | 7.2 | 0 | 6.7 |
| Ab | 0.5 | 0.3 | 0 | 9.3 |
| Ne | 5.41 | 6.7 | 8.2 | 7.7 |
| Le | 0 | 0 | 7.0 | 0 |
| An | 14.2 | 13.9 | 17.8 | 23.0 |
| Wo | 10.7 | 9.6 | 12.1 | 10.0 |
| En | 8.7 | 7.6 | 9.4 | 7.1 |
| Fs | 0.7 | 0.9 | 1.3 | 2.0 |
| Fo | 33.1 | 32.2 | 24.2 | 15.6 |
| Fa | 2.8 | 4.1 | 3.9 | 4.9 |
| ∑ | 94.91 | 94.2 | 94.7 | 95.2 |

But they form small prismatic grains in the dark black main mass (Fig 4). In some cases, besides the microscopic research, according to the results of microprobe analysis (Table 4), the composition of those rhombic and monoclinic pyroxenes is less variable compared to each other. So, the quantitative behaviors of the mineral-forming components in rhombic pyroxenes are really close to each other (Table 4, an. 3, 5, 10, 73). At the same time, the values of the magnesium coefficient are slightly different from each other (Mg#=0.80-0.85). Monoclinic pyroxenes are also homogeneous, their composition differs a little from each other (Table 4). One of their most characteristic features is that titanium, sodium and aluminum oxides from the mineral-forming components are low-grade. But they are rich in silicon and magnesium oxides. Trivalent iron fills aluminum deficiencies in the IV coordination of monoclinic pyroxenes while calculating crystallochemical formulas. As a direct consequence of this, aluminum does not participate in the VI coordination. Calcium chermak minal is almost absent in the minal composition calculated by the Kushiro method (Kushiro, 1965). According to the existing classifications (Добрецов и др., 1971; Morimoto, 1988) the rhombic pyroxenes of the Upper Jurassic picrites of the Murovdag anticlinorium are bronzite-bearing, and the monoclinic pyroxenes are mainly chromium-bearing diopside.

Crystallization temperature of rhombic and monoclinic pyroxenes are 820ºC and 900-1000ºC (Table 4, Fig. 5) according to Lindsley (Lindsley, 1983) paleothermometer.

The Upper Jurassic picrites of the Murovdag anticlinorium were formed under similar geological and geodynamic conditions, while being controlled by the rift-type fault structure. Therefore, the rocks of petrographic type in the composition of picrites are homogeneous. The pyroxenes of these evolved picrites are closely related in terms of mineralogy, crystallization temperature and end-members compositions.

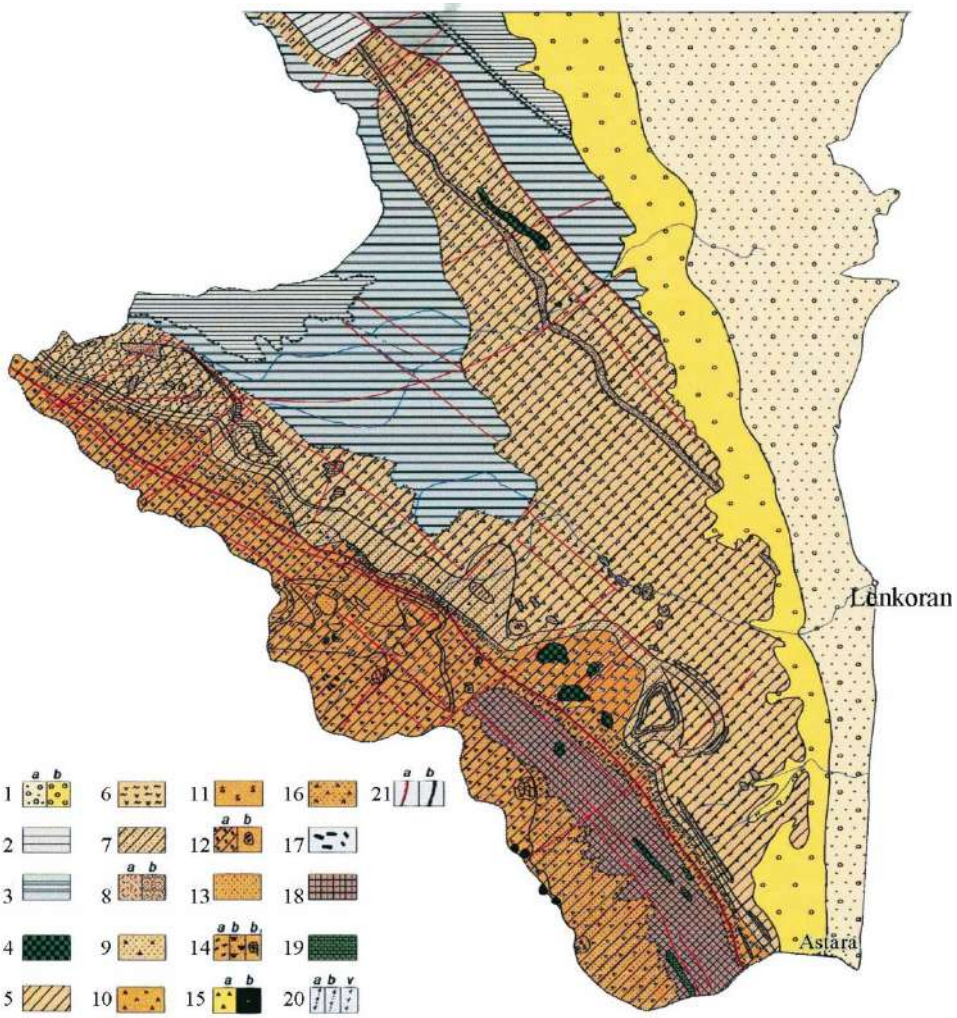


**Fig. 3.** Structural-formation map of the Talysh zone

1 – the Quaternary sediments: a) the Holocene sediments, b) the Pleistocene sediments; 2 – the Upper mollasse sediments (the Middle and the Upper Pliocene); 3 – the Lower mollasse sediments (the Oligocene and Upper Miocene); 4 – the subalkaline ultrabasic formation (the Upper Eocene-Lower Oligocene); the Eocene trachybasalt-trachyandezibasalt-phonolite formation; 5 – the trachybasalt-trachyandezibasalt (latite)-phonolite complex (the Upper Eocene); 6 – the layer of tuffaceous sandstones; 7 – the leucitic phonolite layer; 8 – the subalkaline trachybasalts, layer of trachydolerites: a) lava, pyroclastic facies, b) subvolcanic facies; 9 – the plagioporphyric trachyandezibasalt (latite) layer; 10 – the absarocite-shoshonite-alkaline basalt complex (the Lower-Middle Eocene); 11 – the layer of sedimentary sandstones with flysch tuff; 12 – the alkaline basalts layer: a) lava, pyroclastic facies; b) subvolcanic facies; 13 – the layer of tuffaceous sedimentary sandstones; 14 – the layer of absarocites and leucite tephrites: a) lava, pyroclastic facies, b) subvolcanic facies, $b_1$) subvolcanic gabbro-techenites; 15 – the layer of trachybasalts; 16 – the layer of trachyandezibasalt tuffs; 17 – the dikes of trachybasalt, leucite tephrites and absarocites; 18 – the layer of flysch-tuffaceous sandstones (Paleocene); 19 – the limestone layer (the Upper Cretaceous); 20 – the fractures bordering structural floors: a) the Eocene age; b) the Oligocene age; v) the Miocene age; 21 – the magma-carrying and emplacement faults; a) connecting; b) separating.

Clinopyroxenes occur as phenocrysts, normal prismatic and megacrysts in the Santonian trachybasalt-trachydolerite, tephrite-teschenite complexes of the Khojavand synclinorium (0.5x2.5 cm) (Мамедов и др., 2012). Clinopyroxene megacrysts are dark black and are observed irregularly in gray tephrite-bearing breccias. A contact zone is noticeable in its source rock. Elongated prismatic crystals truncated by transverse crack are observed under the microscope. In most cases, fine and partially idiomorphic fine chrome spinel grains occur as inclusions. The subalkaline picrites have low-grade thermal contact with basic rocks. As a result of the microprobe analysis, it was determined that it contains chrome diopside (Table 5). So, diopside molecule is 47.1%, and enstatite is about 45% in its end members. It is located in the area of modal diopside in the classification chart (Fig. 5).Unlike diopsides of normative alkaline picrites of the Murovdag anticlinorium, the concentration of aluminum and chromium is here significantly increased. If we compare the subalkaline picrites of the described megacrysts with the central part (Fig. 6a) of the zoned pyroxenes in the picrotephrites, it is observed that they have a similar composition (Table 5, an. 1).

***Table 3***

Chemical and normative mineralogical compositions of picrites of the Talysh zone

| an. / Komp. | 1 | 2 | 3 | 4 | 5 | 6 | 7 | 8 | 9 | 10 | 11 |
|---|---|---|---|---|---|---|---|---|---|---|---|
| $SiO_2$ | 41.4 | 41.50 | 41.82 | 41.57 | 41.62 | 41.88 | 41.9 | 42.8 | 42.6 | 43.47 | 43.64 |
| $TiO_2$ | 0.53 | 0.59 | 0.5 | 0.4 | 0.37 | 0.44 | 0.69 | 0.4 | 0.55 | 0.61 | 0.78 |
| $Al_2O_3$ | 6.32 | 6.31 | 5.65 | 5.53 | 5.63 | 5.91 | 7.92 | 9.39 | 12.16 | 12.40 | 12.26 |
| $Fe_2O_3$ | 4.35 | 3.18 | 3.96 | 3.37 | 3.09 | 2.46 | 3.23 | 3.16 | 3.21 | 3.78 | 2.36 |
| FeO | 7.45 | 7.64 | 6.7 | 6.23 | 6.4 | 7.72 | 6.56 | 6.32 | 4.12 | 6.20 | 6.16 |
| MnO | 0.14 | 0.18 | 0.2 | 0.18 | 0.18 | 0.19 | 0.19 | 0.18 | 0.16 | 0.24 | 0.24 |
| MgO | 24.76 | 25.6 | 26.5 | 25.75 | 26.01 | 24.75 | 20.34 | 16.55 | 16.25 | 14.20 | 14.10 |
| CaO | 5.45 | 5.94 | 5.21 | 7.8 | 8.79 | 7.98 | 10.32 | 11.34 | 11.9 | 10.23 | 11.16 |
| $Na_2O$ | 1.46 | 1.56 | 1.46 | 1.52 | 1.24 | 1.52 | 1.86 | 1.91 | 1.46 | 1.38 | 1.38 |
| $K_2O$ | 1.72 | 1.78 | 1.69 | 1.63 | 0.92 | 1.1 | 1.2 | 1.79 | 1.26 | 1.46 | 1.64 |
| $P_2O_5$ | 0.21 | 0.15 | 0.2 | 0.21 | 0.18 | 0.14 | 0.15 | 0.18 | 0.12 | - | - |
| LOI | 5.7 | 5.46 | 5.94 | 5.6 | 5.42 | 5.35 | 5.55 | 5.88 | 5.64 | 5.68 | 6.20 |
| ∑ | 99.49 | 99.89 | 99.83 | 99.79 | 99.85 | 99.44 | 99.91 | 99.9 | 99.43 | 99.65 | 99.92 |
| Ap | 0.3 | 0.3 | 0.3 | 0.3 | 0.3 | 0.3 | 0.3 | 0.3 | 0.1 | - | - |
| Il | 0.9 | 1.1 | 0.9 | 0.8 | 0.6 | 0.9 | 1.4 | 0.8 | 0.9 | 1.1 | 1.5 |
| Mt | 6.3 | 4.6 | 5.9 | 4.9 | 4.4 | 3.5 | 4.6 | 4.6 | 4.6 | 5.1 | 3.5 |
| Or | 10 | 10.6 | 10.0 | 4.2 | 4.2 | 6.7 | 3.3 | 4.5 | 7.2 | 8.3 | 9.5 |
| Ab | 5.0 | 0.9 | 4.7 | - | - | 0.7 | - | - | 1.4 | 10.0 | 4.6 |
| An | 4.3 | 5.0 | 3.3 | 3.6 | 7.0 | 5.8 | 9.7 | 11.7 | 22.8 | 23.6 | 22.5 |
| Ne | 4.1 | 6.7 | 4.3 | 2.7 | 5.7 | 6.7 | 8.5 | 8.8 | 6.0 | 0.8 | 3.8 |
| Le | - | - | - | 4.1 | 1.1 | - | 3.1 | 5.3 | - | - | - |
| Wo | 8.6 | 9.8 | 8.2 | 14.3 | 14.9 | 13.7 | 17.0 | 18.2 | 14.7 | 11.4 | 13.7 |
| En | 6.6 | 7.4 | 7.1 | 11.2 | 11.6 | 10.3 | 12.9 | 13.6 | 11.8 | 8.4 | 10.0 |
| Fs | 1.1 | 1.3 | 0.9 | 1.5 | 1.6 | 2.0 | 2.2 | 2.9 | 1.2 | 1.8 | 2.4 |
| Fo | 38.6 | 39.5 | 41.2 | 37.0 | 37.2 | 35.9 | 26.4 | 19.4 | 20.0 | 18.9 | 17.6 |
| Fa | 6.6 | 7.2 | 6.5 | 5.3 | 5.6 | 7.6 | 4.9 | 4.5 | 2.3 | 3.3 | 4.5 |

1, 2, 3, 4 – subalkaline olivine picrites, porphyritic; 5, 6, 7 – subalkaline olivine-clinopyroxene picrites, porphyritic; 8, 9 – subalkaline olivine-clinopyroxene-plagioclase picrites, porphyritic; 10, 11 – subalkaline clinopyroxene-plagioclase picrites

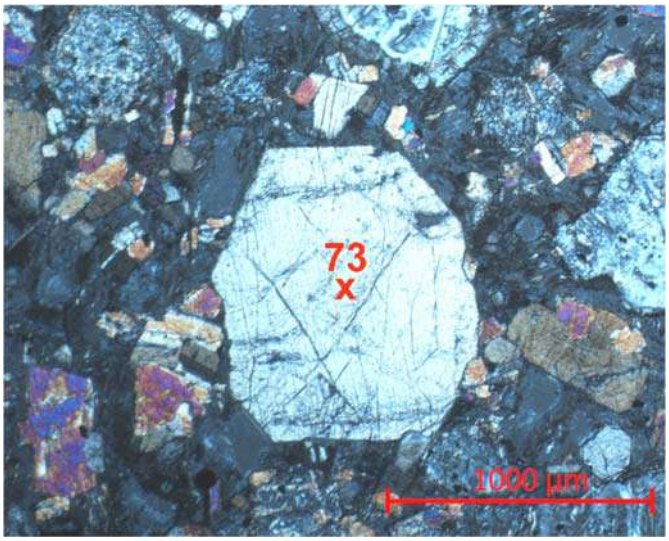


**Fig. 4.** Clinopyroxene phenocrystal in olivine picrite

***Table 4***

Chemical compositions, crystallochemical and end-members of pyroxenes of the Murovdag anticlinorium

| minerals | clinopyroxene | | | | | | | | orthopyroxene | | | |
|---|---|---|---|---|---|---|---|---|---|---|---|---|
| an. / komp. | 3 | 5 | 10 | 73 | 72 | 74 | 76 | 79 | 3 | 5 | 10 | 73 |
| $SiO_2$ | 52.56 | 52.60 | 51.60 | 52.46 | 51.08 | 51.90 | 52.48 | 50.16 | 54.62 | 54.65 | 55.38 | 54.26 |
| $TiO_2$ | 0.42 | 0.34 | 0.38 | 0.28 | 0.48 | 0.16 | 0.29 | 0.46 | 0.30 | 0.23 | 0.16 | 0.16 |
| $Al_2O_3$ | 1.41 | 1.52 | 1.41 | 0.85 | 2.63 | 1.76 | 1.46 | 3.40 | 0.85 | 0.82 | 0.54 | 1.20 |
| $Cr_2O_3$ | 0.54 | 0.63 | 0.74 | 0.68 | 0.32 | 0.72 | 0.64 | 0.16 | 0.52 | 0.58 | 0.39 | 0.39 |
| $Fe_2O_3$ | 1.08 | 0.86 | 2.56 | 1.28 | 3.87 | 2.36 | 2.36 | 5.55 | 2.46 | 1.80 | 0.90 | 3.13 |
| FeO | 4.99 | 6.01 | 4.90 | 5.75 | 3.93 | 4.08 | 4.03 | 2.31 | 8.62 | 10.23 | 9.65 | 7.32 |
| MnO | 0.34 | 0.16 | 0.22 | 0.16 | 0.06 | 0.12 | 0.16 | 0.12 | 0.23 | 0.16 | 0.25 | 0.14 |
| MgO | 16.82 | 16.38 | 16.12 | 16.80 | 16.10 | 16.45 | 16.74 | 16.08 | 31.12 | 29.89 | 30.70 | 31.25 |
| NiO | 0.21 | 0.24 | 0.18 | 0.18 | 0.10 | 0.24 | 0.24 | 0.12 | 0.10 | 0.28 | 0.46 | 0.30 |
| CoO | 0.16 | 0.19 | 0.16 | 0.21 | 0.08 | 0.12 | 0.18 | 0.07 | 0.12 | 0.16 | 0.34 | 0.28 |
| CaO | 21.16 | 20.70 | 21.10 | 20.06 | 21.20 | 21.10 | 20.82 | 21.30 | 0.86 | 1.30 | 0.69 | 1.35 |
| $Na_2O$ | 0.12 | 0.22 | 0.21 | 0.20 | 0.34 | 0.28 | 0.42 | 0.40 | - | - | - | - |
| ∑ | 99.81 | 99.85 | 99.58 | 98.91 | 100.19 | 99.29 | 99.82 | 100.13 | 99.8 | 100.1 | 99.46 | 99.78 |
| tºC | 900 | 900 | 900 | 1000 | 880 | 880 | 900 | 820 | | | | |
| Mg# | 0.83 | 0.81 | 0.80 | 0.80 | 0.79 | 0.82 | 0.83 | 0.80 | 0.84 | 0.82 | 0.84 | 0.85 |
| T | | | | | | | | | | | | |
| Si | 1.939 | 1.944 | 1.918 | 1.950 | 1.882 | 1.926 | 1.933 | 1.849 | | | | |
| Al | 0.061 | 0.056 | 0.061 | 0.037 | 0.114 | 0.074 | 0.063 | 0.147 | | | | |
| $Fe^{+3}$ | - | - | 0.021 | 0.013 | 0.004 | - | 0.004 | 0.004 | | | | |
| M1 | | | | | | | | | | | | |
| Al | - | 0.010 | - | - | - | 0.001 | - | - | | | | |
| $Fe^{+3}$ | 0.030 | 0.024 | 0.050 | 0.024 | 0.104 | 0.066 | 0.062 | 0.15 | | | | |
| Ti | 0.012 | 0.009 | 0.011 | 0.008 | 0.013 | 0.004 | 0.008 | 0.013 | | | | |
| Cr | 0.015 | 0.018 | 0.022 | 0.020 | 0.009 | 0.021 | 0.019 | 0.004 | | | | |
| Mg | 0.800 | 0.769 | 0.775 | 0.779 | 0.764 | 0.787 | 0.792 | 0.765 | | | | |
| $Fe^{+2}$ | 0.133 | 0.158 | 0.132 | 0.160 | 0.105 | 0.110 | 0.107 | 0.062 | | | | |
| Ni | 0.006 | 0.007 | 0.005 | 0.005 | 0.003 | 0.007 | 0.007 | 0.004 | | | | |
| Co | 0.004 | 0.006 | 0.005 | 0.006 | 0.002 | 0.004 | 0.005 | 0.002 | | | | |
| M2 | | | | | | | | | | | | |
| $Fe^{+2}$ | 0.021 | 0.027 | 0.020 | 0.031 | 0.016 | 0.017 | 0.017 | 0.009 | | | | |
| Mg | 0.124 | 0.133 | 0.118 | 0.151 | 0.120 | 0.121 | 0.127 | 0.118 | | | | |
| Mn | 0.011 | 0.005 | 0.007 | 0.005 | 0.002 | 0.004 | 0.005 | 0.004 | | | | |
| Ca | 0.836 | 0.819 | 0.840 | 0.799 | 0.837 | 0.838 | 0.823 | 0.844 | | | | |
| Na | 0.008 | 0.016 | 0.015 | 0.014 | 0.025 | 0.020 | 0.029 | 0.029 | | | | |
| | | | | | | | | | | | | |
| Si | 1.939 | 1.944 | 1.918 | 1.950 | 1.882 | 1.926 | 1.933 | 1.847 | 1.933 | 1.944 | 1.973 | 1.920 |
| Ti | 0.012 | 0.009 | 0.011 | 0.008 | 0.013 | 0.004 | 0.008 | 0.013 | 0.008 | 0.006 | 0.004 | 0.004 |
| Al | 0.061 | 0.066 | 0.061 | 0.037 | 0.114 | 0.075 | 0.063 | 0.148 | 0.035 | 0.034 | 0.023 | 0.050 |
| Cr | 0.015 | 0.018 | 0.022 | 0.020 | 0.009 | 0.021 | 0.019 | 0.004 | 0.015 | 0.016 | 0.011 | 0.011 |
| $Fe^{+3}$ | 0.030 | 0.024 | 0.071 | 0.035 | 0.108 | 0.066 | 0.066 | 0.154 | 0.066 | 0.048 | 0.024 | 0.083 |
| $Fe^{+2}$ | 0.154 | 0.186 | 0.152 | 0.191 | 0.121 | 0.127 | 0.124 | 0.071 | 0.255 | 0.304 | 0.288 | 0.217 |
| Mn | 0.011 | 0.005 | 0.007 | 0.005 | 0.002 | 0.004 | 0.005 | 0.004 | 0.007 | 0.005 | 0.008 | 0.004 |
| Mg | 0.924 | 0.901 | 0.893 | 0.930 | 0.884 | 0.908 | 0.919 | 0.883 | 1.642 | 1.585 | 1.631 | 1.649 |
| Ni | 0.006 | 0.007 | 0.005 | 0.005 | 0.003 | 0.007 | 0.007 | 0.003 | 0.003 | 0.003 | 0.003 | 0.003 |
| Co | 0.004 | 0.006 | 0.005 | 0.006 | 0.002 | 0.004 | 0.005 | 0.002 | 0.003 | 0.005 | 0.010 | 0.008 |
| Ca | 0.836 | 0.819 | 0.840 | 0.799 | 0.837 | 0.838 | 0.823 | 0.841 | 0.033 | 0.050 | 0.026 | 0.051 |
| Na | 0.008 | 0.016 | 0.015 | 0.014 | 0.025 | 0.020 | 0.029 | 0.030 | - | - | - | - |
| ∑ | 4.000 | 4.000 | 4.000 | 4.000 | 4.000 | 4.000 | 4.000 | 4.000 | 4.000 | 4.000 | 4.000 | 4.000 |

| End-members | | | | | | | | | | | | |
|---|---|---|---|---|---|---|---|---|---|---|---|---|
| $NaFe^{+3}Si_2O_6$ | 0.9 | 1.6 | 1.5 | 1.4 | 2.5 | 2.0 | 2.9 | 3.0 | | | | |
| $CaTiAl_2O_6$ | 1.2 | 1.0 | 1.1 | 0.8 | 1.3 | 0.4 | 0.8 | 1.3 | | | | |
| $CaAl_2SiO_6$ | 0.4 | 1.5 | 2.1 | 1.3 | 0.4 | 0.3 | 0.4 | 0.5 | | | | |
| CaFeAlSi | 3.7 | 2.7 | 3.6 | 1.8 | 8.6 | 6.7 | 4.7 | 12.0 | | | | |
| $Ca_2Si_2O_6$ | 39.3 | 38.5 | 38.6 | 37.9 | 36.6 | 38.3 | 38.2 | 35.1 | | | | |
| $Mg_2Si_2O_6$ | 46.3 | 45.2 | 45.2 | 47.0 | 44.4 | 45.8 | 46.5 | 44.4 | | | | |
| $Fe_2Si_2O_6$ | 8.2 | 9.6 | 7.9 | 9.8 | 6.2 | 6.5 | 6.5 | 3.7 | | | | |
| $MgSiO_3$ | 42.8 | 42.3 | 42.8 | 40.7 | 42.9 | 43.1 | 42.5 | 43.1 | 1.7 | 2.6 | 1.4 | 2.7 |
| $CaSiO_3$ | 47.2 | 46.6 | 45.5 | 47.4 | 45.3 | 46.7 | 47.4 | 45.2 | 85.1 | 81.7 | 83.8 | 86.0 |
| $FeSiO_3$ | 10.0 | 11.1 | 11.7 | 11.9 | 11.8 | 10.2 | 10.1 | 11.7 | 13.2 | 15.7 | 14.8 | 11.3 |

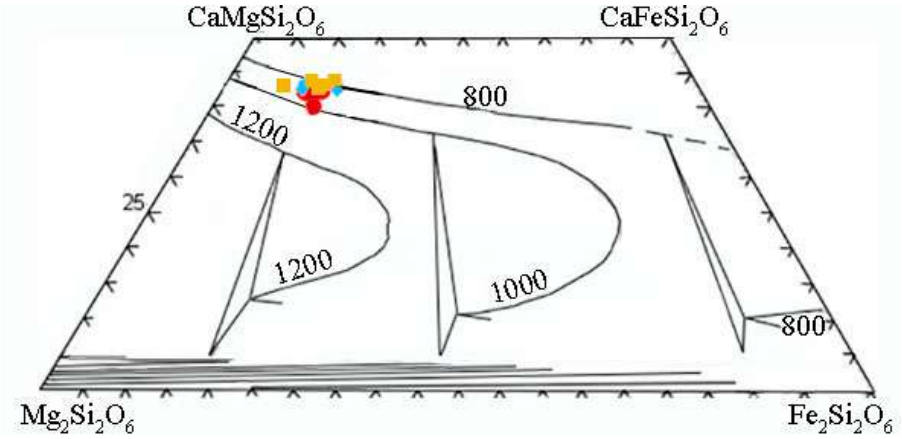


**Fig. 5.** Pyroxene compositions on the Di-Hd-En-Fs diagram (Lindsley, 1983; Rohrbach et al., 2005)

The concentrations of enstatite and diopside molecules are close to each other in the central part of zoned diopsides (Table 5, an. 2) (Fig. 6b). At the same time, the concentrations of chromium and aluminum oxides are relatively high here as in megacrysts.

The amount of aluminum oxide remains constant, while the amount of chromium and titanium gradually decreases from the center of the zoned crystals to the outside, i.e. under conditions of calcium dominance (CaO=23.20%) in the next zone (Table 5, an. 3) (Fig. 6b).

The clinopyroxenes in the composition of picrothechenites are prismatic, and the amount of silicon, chromium, and magnesium oxides in their composition decreases sharply. The amount of titanium and aluminum oxides increases significantly. The amount of calcium and iron oxides remains relatively constant. Essenite ($CaFe^{+3}AlSiO_6$) molecule increases in the composition of the end members.

An increase in aluminum and titanium oxides in the composition of clinopyroxenes is also observed in picrotephrites. The concentration of calcium oxide in mineral-forming clinopyroxenes is less variable.

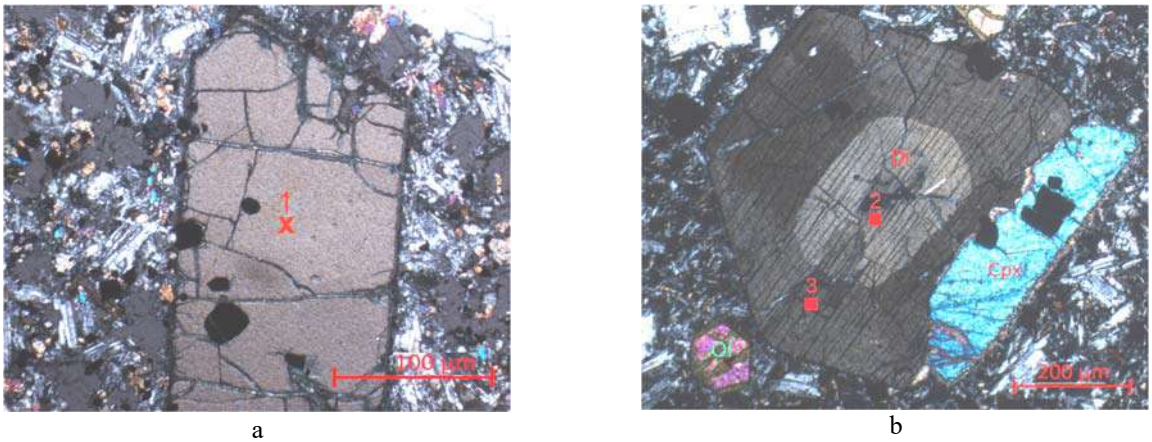


a b

**Fig. 6.** a – zoned pyroxene phenocryst in picrotefrite; b – pyroxene megacrystal in picrotefrite

***Table 5***

Chemical, crystallochemical compositions and end-members of pyroxenes of the Khojavand synclinorium

| an. / komp. | | 1 | 2 | 3 | 4 |
|---|---|---|---|---|---|
| $SiO_2$ | | 51.60 | 51.30 | 51.20 | 51.87 |
| $TiO_2$ | | 0.37 | 0.45 | 1.17 | 0.22 |
| $Al_2O_3$ | | 2.67 | 2.67 | 3.36 | 2.31 |
| $Cr_2O_3$ | | 1.20 | 1.16 | 0.76 | 0.21 |
| $Fe_2O_3$ | | 0.95 | 2.15 | 1.09 | 2.15 |
| FeO | | 4.18 | 3.71 | 4.23 | 4.83 |
| MnO | | 0.11 | 0.16 | 0.24 | 0.12 |
| MgO | | 15.44 | 16.07 | 15.46 | 14.53 |
| CaO | | 22.60 | 22.2 | 22.20 | 23.2 |
| $Na_2O$ | | 0.32 | 0.16 | 0.38 | 0.36 |
| ∑ | | 99.44 | 100.03 | 100.09 | 99.8 |
| Mg# | | 0.83 | 0.83 | 0.77 | 0.76 |
| tºC | | 820 | 840 | 780 | 820 |
| Cations in T, M1, M2 positions | | | | | |
| T | Si | 1.907 | 1.888 | 1.862 | 0.923 |
| | Al | 0.093 | 0.112 | 0.138 | 0.077 |
| $M_1$ | Al | 0.027 | 0.006 | 0.009 | 0.024 |
| | $Fe^{+3}$ | 0.026 | 0.059 | 0.030 | 0.060 |
| | Ti | 0.010 | 0.012 | 0.033 | 0.006 |
| | Cr | 0.035 | 0.034 | 0.022 | 0.006 |
| | Mg | 0.783 | 0.787 | 0.786 | 0.762 |
| | $Fe^{+2}$ | 0.119 | 0.102 | 0.120 | 0.142 |
| $M_2$ | $Fe^{+2}$ | 0.010 | 0.012 | 0.011 | 0.008 |
| | Mg | 0.068 | 0.096 | 0.072 | 0.041 |
| | Mn | 0.003 | 0.005 | 0.007 | 0.004 |
| | Ca | 0.896 | 0.875 | 0.882 | 0.921 |
| | Na | 0.023 | 0.012 | 0.028 | 0.026 |
| End members | | | | | |
| $NaFe^{+3}Si_2O_6$ | | 2.3 | 1.2 | 2.7 | 2.6 |
| $CaTiAl_2O_6$ | | 1.0 | 1.2 | 3.3 | 0.6 |
| $CaAl_2SiO_6$ | | 2.4 | 0.4 | 0.9 | 2.2 |
| $CaFeAlSiO_6$ | | 3.9 | 8.2 | 2.5 | 4.1 |
| $Ca_2Si_2O_6$ | | 40.3 | 39.6 | 39.6 | 41.4 |
| $Mg_2Si_2O_6$ | | 38.3 | 39.8 | 38.3 | 36.1 |
| $Fe_2Si_2O_6$ | | 6.4 | 7.9 | 7.6 | 9.6 |
| $CaSiO_3$ | | 42.9 | 43.9 | 43.8 | 43.0 |
| $MgSiO_3$ | | 47.7 | 46.8 | 43.1 | 43.6 |
| $FeSiO_3$ | | 9.4 | 9.4 | 13.1 | 13.5 |

The clinopyroxenes in the Santonian picrites and picrothechenites of the Khojavand synclinorium correspond to chrome, partially aluminum diopsides. According to Lindsley paleothermometer, their crystallization temperature ranges between 780-840ºC (Table 5, Fig. 5). The chromium diopside megacryst has been formed as an accumulative inclusion. Therefore, it corresponds to the central part of the zoned crystals. At the same time, the absence of a thermal break between the zones of the zoned clinopyroxenes and the gradual alteration of clinopyroxene composition in the zones show that this process is regulated by crystallization differentiation. In this direction, crystallization temperature is also characterized by a gradual alteration.

The increase of titanium and aluminum oxides, the decrease of magnesium and chromium oxides are confirmed by the alteration of the modal mineralogical composition of the subalkaline picrites due to the partial intense fractionation in the last rim of the zoned crystals. So, chromium diopside is gradually replaced by salite, calcium augite and chrome spinel by chrome-magnetite.

Picrites belong to the subalkaline series and have a characteristic impregnation structure and their main masses are dolerite and subdolerite structured in the Talysh zone (Мамедов и др., 2017). Besides olivine, clinopyroxene phenocrysts are present in the impregnations. In most cases, those phenocrysts form large elongated, sometimes plate-like crystals. In most cases, they are colorless. However, olivine and chrome spinel inclusions of different sizes are observed in them. Relatively large prismatic phenocrysts (1.5-2.3 cm) of clinopyroxenes occur in phlogopite and olivine picrites. These phenocrysts are xenomorphic compared to olivine. According to their chemical composition (Table 6), these megacrysts are partial high-grade in magnesium, silicon and chrome oxides, and low-grade in aluminum and titanium oxides. This composition diversity is also reflected in the calculation of compositions of the end members. So, the concentration of enstatite in the composition of the abovementioned phenocrysts ranges between 42.0-46.8%. Correspondingly, titanium and calcium chermak molecules decrease significantly (Table 6, an. 1). According to Lindsley thermometer (Lindsley, 1983), the crystallization temperature of these phenocrysts ranges from 700 to 900°C (Table 6, Fig. 5).

The second group of clinopyroxene phenocrysts has a characteristic prismatic shape, and in most cases has a zoned structure.

***Table 6***

Chemical, crystallochemical compositions of clinopyroxenes in picrites of the Talysh zone

| | | 1 | 2 | 3 | 4 | 5 | 6 | 7 | 8 | 9 | 10 | 11 | 12 |
|---|---|---|---|---|---|---|---|---|---|---|---|---|---|
| | $SiO_2$ | 51.90 | 50.41 | 50.25 | 50.60 | 51.50 | 50.63 | 51.76 | 51.24 | 51.26 | 48.92 | 49.40 | 49.36 |
| | $TiO_2$ | 0.16 | 0.53 | 0.73 | 0.41 | 0.41 | 0.58 | 0.43 | 0.66 | 0.75 | 0.64 | 0.61 | 0.53 |
| | $Al_2O_3$ | 3.33 | 3.63 | 3.47 | 4.16 | 3.24 | 3.15 | 2.23 | 2.89 | 3.12 | 5.26 | 4.80 | 4.78 |
| | $Cr_2O_3$ | 0.89 | 0.65 | 0.50 | 0.75 | 0.62 | 0.62 | 0.63 | 0.42 | 0.15 | 0 | 0 | 0 |
| | $Fe_2O_3$ | 2.26 | 3.87 | 3.42 | 2.14 | 1.73 | 3.86 | 2.37 | 1.93 | 1.94 | 3.81 | 4.24 | 3.80 |
| | FeO | 2.17 | 4.03 | 2.69 | 4.73 | 3.12 | 4.47 | 3.59 | 3.05 | 4.46 | 5.69 | 4.52 | 5.38 |
| | MnO | 0.16 | 0.16 | 0.14 | 0.15 | 0.06 | 0.19 | 0.15 | 0.12 | 0.18 | 0.16 | 0.14 | 0.20 |
| | MgO | 16.93 | 15.50 | 15.15 | 15.40 | 16.32 | 15.20 | 15.98 | 15.48 | 15.66 | 13.41 | 13.46 | 13.42 |
| | CaO | 21.97 | 21.10 | 23.00 | 21.20 | 22.45 | 21.64 | 22.36 | 23.4 | 21.75 | 21.42 | 22.30 | 21.66 |
| | $Na_2O$ | 0.36 | 0.39 | 0.34 | 0.26 | 0.21 | 0.35 | 0.29 | 0.26 | 0.40 | 0.46 | 0.54 | 0.46 |
| | Mg# | 0.87 | 0.79 | 0.82 | 0.80 | 0.86 | 0.77 | 0.83 | 0.85 | 0.82 | 0.72 | 0.74 | 0.73 |
| | tºC | 880 | 800 | 800 | 900 | 780 | 800 | 800 | 860 | 800 | 820 | 750 | 700 |
| | ∑ | 100.13 | 100.27 | 99.69 | 99.5 | 99.66 | 100.69 | 99.79 | 99.45 | 99.67 | 99.77 | 100.01 | 99.59 |
| Cations in T, M1, M2 positions | | | | | | | | | | | | | |
| T | Si | 1.893 | 1.859 | 1.860 | 1.869 | 1.893 | 1.865 | 1.909 | 1.895 | 1.893 | 1.920 | 1.921 | 1.893 |
| | Al | 0.107 | 0.141 | 0.140 | 0.131 | 0.107 | 0.135 | 0.091 | 0.105 | 0.107 | 0.080 | 0.079 | 0.107 |
| $M_1$ | Al | 0.036 | 0.017 | 0.011 | 0.050 | 0.033 | 0.002 | 0.006 | 0.021 | 0.029 | 0.049 | 0.040 | 0.013 |
| | $Fe^{+3}$ | 0.062 | 0.107 | 0.095 | 0.060 | 0.048 | 0.106 | 0.066 | 0.054 | 0.055 | 0.019 | 0.036 | 0.095 |
| | Ti | 0.004 | 0.015 | 0.020 | 0.011 | 0.011 | 0.016 | 0.012 | 0.018 | 0.021 | 0.012 | 0.016 | 0.012 |
| | Cr | 0.026 | 0.019 | 0.015 | 0.022 | 0.018 | 0.018 | 0.018 | 0.012 | 0.004 | - | - | - |
| | Mg | 0.809 | 0.730 | 0.778 | 0.731 | 0.804 | 0.736 | 0.797 | 0.806 | 0.770 | 0.699 | 0.688 | 0.717 |
| | $Fe^{+2}$ | 0.063 | 0.112 | 0.081 | 0.126 | 0.086 | 0.122 | 0.101 | 0.089 | 0.122 | 0.211 | 0.220 | 0.163 |
| $M_2$ | $Fe^{+2}$ | 0.003 | 0.013 | 0.002 | 0.020 | 0.010 | 0.016 | 0.010 | 0.005 | 0.015 | 0.021 | 0.019 | 0.012 |
| | Mg | 0.111 | 0.121 | 0.057 | 0.116 | 0.089 | 0.099 | 0.081 | 0.045 | 0.091 | 0.072 | 0.059 | 0.052 |
| | Mn | 0.005 | 0.005 | 0.004 | 0.005 | 0.002 | 0.006 | 0.005 | 0.004 | 0.006 | 0.006 | 0.006 | 0.009 |
| | Ca | 0.856 | 0.833 | 0.912 | 0.839 | 0.884 | 0.855 | 0.883 | 0.927 | 0.860 | 0.879 | 0.886 | 0.901 |
| | Na | 0.025 | 0.028 | 0.025 | 0.019 | 0.015 | 0.024 | 0.021 | 0.019 | 0.028 | 0.022 | 0.030 | 0.026 |

| End members | 1 | 2 | 3 | 4 | 5 | 6 | 7 | 8 | 9 | 10 | 11 | 12 |
|---|---|---|---|---|---|---|---|---|---|---|---|---|
| $NaFe^{+3}Si_2O_6$ | 2.5 | 2.8 | 2.4 | 1.9 | 1.5 | 2.5 | 2.1 | 1.9 | 2.9 | 2.2 | 3.0 | 2.6 |
| $CaTiAl_2O_6$ | 0.4 | 1.5 | 2.0 | 1.1 | 1.1 | 1.6 | 1.2 | 1.8 | 2.1 | 1.2 | 1.6 | 1.2 |
| $CaAl_2SiO_6$ | 3.4 | 1.6 | 1.0 | 5.0 | 3.3 | 0.2 | 0.6 | 2.0 | 2.7 | 4.7 | 4.0 | 1.3 |
| CaFeAlSi | 6.2 | 9.8 | 8.5 | 6.3 | 5.1 | 10.0 | 6.3 | 4.4 | 3.0 | 0.8 | 0.6 | 7.0 |
| $Ca_2Si_2O_6$ | 39.1 | 37.6 | 41.0 | 37.8 | 40.0 | 38.6 | 39.9 | 41.7 | 38.8 | 38.2 | 39.8 | 38.6 |
| $Mg_2Si_2O_6$ | 42.0 | 38.4 | 37.6 | 38.2 | 40.5 | 37.7 | 39.6 | 38.4 | 38.8 | 33.3 | 33.4 | 33.3 |
| $Fe_2Si_2O_6$ | 6.1 | 10.7 | 8.2 | 9.5 | 6.5 | 11.3 | 8.0 | 6.7 | 7.7 | 10.5 | 9.1 | 10.2 |
| $CaSiO_3$ | 43.7 | 43.4 | 44.0 | 42.2 | 46.0 | 44.0 | 45.5 | 43.5 | 44.8 | 42.0 | 46.8 | 45.8 |
| $MgSiO_3$ | 49.9 | 44.3 | 45.8 | 44.7 | 46.4 | 43.0 | 45.2 | 47.8 | 45.0 | 39.0 | 39.3 | 39.4 |
| $FeSiO_3$ | 7.4 | 12.3 | 10.2 | 11.1 | 7.6 | 13.0 | 9.3 | 8.7 | 10.2 | 19.0 | 13.9 | 14.8 |

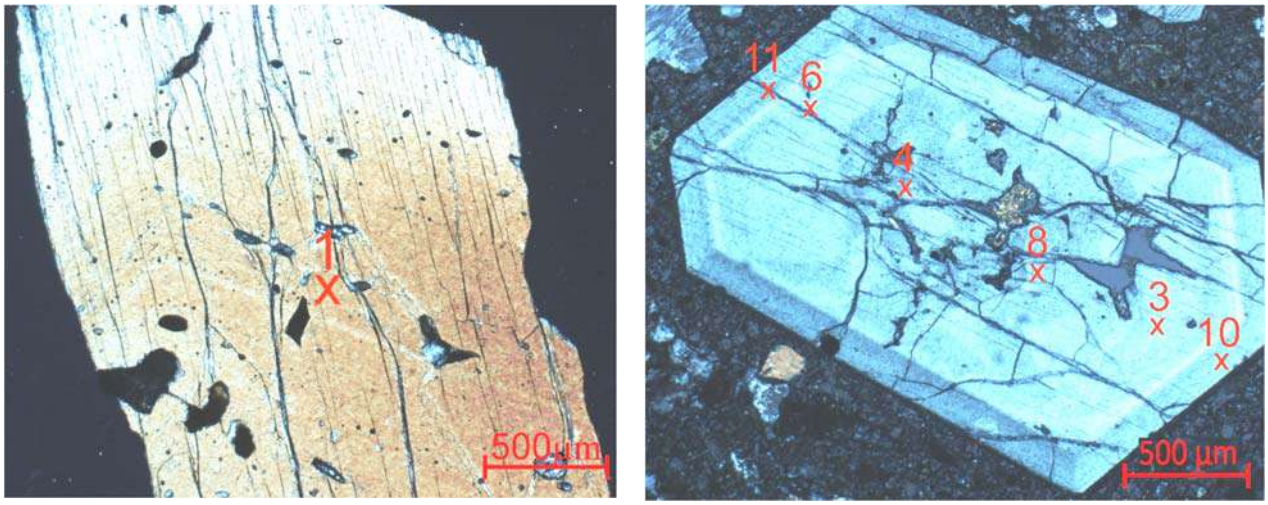


**Fig. 7.** a – pyroxene phenocryst in pycrite; b – zoned pyroxene phenocryst in pycrite

At the same time, the non-zoned phenocrysts are also found (Table 6, an. 1) (Fig. 7a). The compositions of the central part of the zoned prismatic clinopyroxene grains are almost completely similar to those phenocrysts. So, while the relative dominance of silicon and magnesium oxides in phenocrysts remains constant, the amount of aluminum oxide decreases. As a result of such decrease, the amount of calcium chermak molecule also decreases. The calcium chermak molecule partially increases, and the wollastonite molecule decreases in the composition of the end members (Table 6, an. 4, 8) in analysis of the central part of the zoned clinopyroxenes (Fig. 7b).

The transition of the zoned clinopyroxene grain to the next zone is gradual (Table 6, an. 6, 3) (Fig. 7b). The analysis of the composition of this zone shows that the concentrations of aluminum and iron oxides increase significantly, while the amount of silicon oxide decreases. Due to their minal composition, they correspond to diopside-salite. They are located in the area of diopside in the classification chart. Crystallization temperature ranges between 700-900°C (Table 6, Fig. 5).

The result of the analysis of the next rim of the zoned prismatic clinopyroxene shows that the concentration of iron oxide is slightly increased here. As a result, the ferrosilite molecule in the composition of this rim increases weakly, and the calcium chermak minal decreases sharply due to the decrease in the amount of silicon and calcium oxides ($CaAl_2SiO_6$=0.2%).

Finally, the amount of silicon and magnesium oxides in the last rim (Table 6, an. 10, 11 , Fig. 7b) of the zoned clinopyroxene phenocryst decreases significantly, while the amount of aluminum and iron oxides increases due to the gradual transition of the subalkaline olivine and clinopyroxene picrites to the subalkaline plagioclase picrites (Fig. 7b). Therefore, calcium chermak and ferrosilite molecules increase slightly. Calcium chermak and ferrosilite molecules gradually increase in the non-zoned clinopyroxene phenocrysts in the subalkaline picrobasalts (Table 6, an. 1) (Fig. 7a).

As it can be seen from the presented material, the alteration of the composition of clinopyroxene phenocrysts is related to the evolutionary process of the subalkaline picrite magma. So, the alteration of the composition of the subalkaline picrites is controlled by the effect of crystallization differentiation.

**Results**

So, summarizing the conducted research, the following results can be emphasized:

1. The layered picrites located among the Bajocian-Bathonian volcanites on the northeastern slope of the Murovdag anticlinorium are petrographically and petrochemically homogeneous. These signs of homogeneity are explained by the fact that the compositions of monoclinic and rhombic pyroxenes are similar. At the same time, the similarity of their crystallization temperature allows confirming this point of view. Besides, the partial lack of aluminum oxide in their composition caused the absence of the calcium chermak ($CaAl_2SiO_6$) molecule in the composition of clinopyroxene impregnation.

2. Clinopyroxene megacrysts in the Khojavend flexure contain chrome diopside with partial low-grade titanium oxide as phenocrysts in the subalkaline picrites. In this sense, the central part of the zoned phenocrysts is almost similar with megacrysts in terms of composition. The absence of discreteness and gradual transitions between the zones, as well as the decrease of chromium, magnesium oxides and the increase of aluminum and titanium oxides from the center to the outside can be considered a sign of the regulation of the evolution process of the subalkaline picrite magma by crystallization differentiation.

3. Alteration of primary subalkaline picrite fusion of the subalkaline picrites of the Talysh zone in intermediate magmatic focus was probably regulated by crystallization differentiation. So, forsterite-bearing olivine, magnesium-chrome chrome spinel, phlogopite and chrome diopside crystallized and accumulated in the lower part of the intermediate magmatic focus at the early stage of the crystallization process. The partial alteration in the effects of volatile components in the course of this process led to the formation of zoned phenocrysts and the variations in the components in their composition. The gradual variation shows that the leading factor controlling the process is crystallization differentiation. The decisiveness of this factor is explained by the alteration of the composition of clinopyroxene phenocrysts according to the general evolution of the subalkaline picrite magma.

**REFERENCES**


Azizbekov Sh.A., Bagirov A.E., Veliyev M.M., Ismail-Zade A.D., Nizheradzhe N.S., Emelyanova E.N., Mamedov M.N. et al. Geology and volcanism of Talysh. Nauka. Moscow, 1979, 241 p. (in Russian).

Dobretsov N.L., Kochkin Yu.N., Krivenko A.P., Kutolin V.A. Rock-forming pyroxenes. Nauka. Moscow, 1971, 455 p. (in Russian).

Mamedov M.N. Evolution of alkaline basic magmatism in the structures of the Talysh block (southeastern Azerbaijan). In: Evolution of magmatism of the main structures of the Earth, Moscow, 1983, p. 41 (in Russian).

Mamedov M.N., Babayeva G.J., Sadygov N.M. Clinopyroxenes of trachybasalt-trahydoleryte and tephrite-teschenite complexes of the Khojavend trough. Otechestvennaya geologiya, No. 6, 2012, pp. 48-55 (in Russian).

Mammedov M.N., Babayeva G.J., Kerimov V.M. Clinopyroxenes in formation process of sub-alkalic olivine-basalt magma of the Talysh zone of Caucasus. Uralian Geological Journal, No. 5, 2017, pp. 39-53 (in Russian).

Rustamov M.I. Geodinamics and magmatism of the Caspian-Caucasus segment of the Mediterranean belt of the Phanerozoic. Nafta-Press. Baku, 2019, 543 p. (in Russian).

Shikhalibeyli E.Sh. Geology and minerals of Nagorno-Karabakh of Azerbaijan. Baku, 1994, 284 p. (in Russian).

Kushiro I. Clinopyroxene solid solutions. Part I. The $CaAl_2SiO_2$ component. Jap. J. Geol. Geogr., No. 33, 1962, pp. 213-220.

Le Bas M.J., Le Mitre R.W., Streckeisen A., Zanettin B. A chemical classification of volcanic rocks based on the total alkali-silica (TAS) diagram. J. Petrol., Vol. 27, 1986, pp. 745-750, http://doi.org/10.1093/petrology/27.3.745/.

Lindsley D.H. Pyroxene thermometry. American Mineralogist, Vol. 68(5-6), 1983, pp. 477-493.

Morimoto N. Nomenclature of pyroxenes. Mineralogy and Petrology, Vol. 39, 1988, pp. 55-76, http://dx.doi.org/10.1007/BF01226262.

Rohrbach A., Schuth S., Ballhaus C., Miinker C., Matveev S., Qopoto C. Petrological constraints on the origin of arc picrites, New Georgia Group, Solomon Islands. Contrib Mineral Petrol, No. 149, No. 6, 2005, pp. 685-698, http://doi.org/10.1007/S00410-0675-6.


**ЛИТЕРАТУРА**


Азибеков Ш.А., Багиров А.Э., Велиев М.М., Исмаил-Заде А.Д., Нижерадже Н.Ш., Емельянова Е.Н., Мамедов М.Н. Геология и вулканизм Талыша. Элм. Баку, 1979, 241 с.

Добрецов Н.Л., Кочкин Ю.Н., Кривенко А.П., Кутолин В.А. Породообразующие пироксены. Наука. Москва, 1971, 455 с.

Мамедов М.Н. Эволюция щелочного основного магматизма в структурах Талышского блока (юго-восточный Азербайджан). В сб.: Эволюция магматизма в главнейших структурах Земли, Наука. Москва, 1983, с.41-44.

Мамедов М.Н., Бабаева Г.Д., Садыгов Н.М. Клинопироксены трахибазальт-трахидолеритового и тефрит-тешенитового комплексов Ходжавендского прогиба. Отечественная геология, No. 6, 2012, с. 48-55.

Мамедов М.Н., Бабаева Г.Д., Керимов В.М. Клинопироксены в процессе формирования субщелочной оливин-базальтовой магмы Талышской зоны Кавказа. Уральский геологический журнал, No. 5, 2017, с. 39-53.

Рустамов М.И. Геодинамика и магматизм Каспийско-Кавказского сегмента Средиземноморского пояса в фанерозое. Nafta-Press. Баку, 2019, 543 с.

Шихалибейли Э.Ш. Геология и полезные ископаемые Нагорного Карабаха Азербайджана. Элм. Баку, 1994, 284 с.

Kushiro I. Clinopyroxene solid solutions. Part I. The $CaAl_2SiO_2$ component. Jap. J. Geol. Geogr., Vol. 33, 1962, pp. 213-220.

Le Bas M.J., Le Mitre R.W., Streckeisen A., Zanettin B. A chemical classification of volcanic rocks based on the total alkali-silica (TAS) diagram. J. Petrol., Vol. 27, 1986, pp. 745-750, http://doi.org/10.1093/petrology/27.3.745/.

Lindsley D.H. Pyroxene thermometry. American Mineralogist, Vol. 68(5-6), 1983, pp. 477-493.

Morimoto N. Nomenclature of pyroxenes. Mineralogy and Petrology, Vol. 39, 1988, pp. 55-76, http://dx.doi.org/10.1007/BF01226262.

Rohrbach A., Schuth S., Ballhaus C., Miinker C., Matveev S., Qopoto C. Petrological constraints on the origin of arc picrites, New Georgia Group, Solomon Islands. Contrib Mineral Petrol, Vol. 149, No. 6, 2005, pp. 685-698, http://doi.org/10.1007/S00410-0675-6.

## ПЕТРОГЕНЕТИЧЕСКАЯ РОЛЬ ПИРОКСЕНОВ В ФОРМИРОВАНИИ ПИКРИТОВ МАЛОГО КАВКАЗА И ТАЛЫША

**Мамедов М.Н., Бабаева Г.Дж., Сариев Ф.Х.**
*Министерство науки и образования Азербайджанской Республики, Институт геологии и геофизики, Азербайджан AZ1143, Баку, просп. Г.Джавида, 119*: *gultekin_babayeva@rambler.ru*

***Резюме.*** На основе микрозондового, химического и рентгенодифрактометрического анализов изучены петрогенетические особенности формирования пикритов в зависимости от изменчивости составов клинопироксенов Малого Кавказа и Талышской зоны. Верхнеюрские пикриты Муровдагского антиклинория формировались в сходных геолого-геодинамических условиях, но подчинялись рифтогенному строению трещин. Пироксены этих эволюционировавшихся пикритов близки по минералогическому составу, температурам кристаллизации и «минальному» составу. Мегакристаллы клинопироксена в субщелочных пикритах Ходжавендского прогиба соответствуют хромистому диопсиду, частично обедненному оксидом титана. Клинопироксены участвуют в виде вкрапленников, нормально-призматических и мегакристов (0.5x2.5 см) в составе сантонских трахибазальт-трахидолеритового, тефрит-тешенитового комплексов Ходжавендского прогиба. Мегакристаллы клинопироксена темно-черного цвета наблюдаются неравномерно в серых тефритсодержащих брекчиях. Зона контакта заметна в материнской породе. В Талышской зоне пикриты относятся к субщелочной серии и имеют характерное глинистое строение, а их основная масса представлена долеритом и субдолеритом. Наряду с оливином в составе пикритов присутствуют вкрапленники клинопироксена. Эти фенокристаллы в большинстве случаев образуют крупные удлиненные, иногда пластинчатые кристаллы. В большинстве случаев они бесцветны. Однако в них наблюдаются включения оливина и хромшпинелида разного размера. Довольно крупные призматические вкрапленники клинопироксенов (1.5-2.3 см) присутствуют во флогопитовых и оливиновых пикритах. Эти фенокристаллы ксеноморфны оливину. Состав клинопироксенов в пикритах Талышской зоны соответствует диопсид-салиту. Таким образом, изменение состава пикроксенов в пикритах Малого Кавказа и Талышской зоны регулируется кристаллизационной дифференциацией.

***Ключевые слова:*** *Малый Кавказ, Талышская зона, пикрит, зональный пироксен, кристаллизационная дифференциация*

## KİÇİK QAFQAZIN VƏ TALIŞ ZONASININ PİKRİTLƏRİNİN FORMALAŞMASINDA PİROKSENLƏRİN PETROGENETİK ROLU

**Məmmədov M.N., Babayeva G.C., Sarıyev F.H.**
*Azərbaycan Respublikası Elm və Təhsil Nazirliyi, Geologiya və Geofizika İnstitutu, Azərbaycan AZ1143, Bakı, H. Cavid pr., 119: gultekin56@rambler.ru*

***Xülasə.*** Mikrozond, kimyəvi və rentgen-difraktometrik analizlərlə Kiçik Qafqazın və Talış zonasında klinopiroksenlərin tərkib dəyişkənliyi əsasında pikritlərinin əmələgəlməsinin petrogenetik xüsusiyyətləri öyrənilmişdir. Murovdağ antiklinorisinin üst yura yaşlı pikritləri rift təbiətli qırılma strukturu ilə nəzarətlənməklə bərabər, oxşar geoloji-geodinamik şəraitdə formalaşmışdır. Buna görə də, antiklinorinin tərkiblərində iştirak edən petroqrafik tip süxurlar bircinslidirlər. Bu təkamülə uğramış pikritlərin piroksenləri mineraloji cəhətdən, kristallaşma temperaturlarına və "minal" tərkiblərinə görə çox yaxındır. Xocavənd əyilməsində subqələvi pikritlərdə klinopiroksen meqakristalları titan oksidi ilə qismən kasıblaşmış xrom diopsidə uyğundur. Klinopiroksenlər Xocavənd sinklinorisinin santon yaşlı traxibazalt-traxidolerit, tefrit-teşenit komplekslərinin tərkibində fenokristal, normal prizmatik və meqakristal qismində iştirak edirlər (0,5x2,5 sm). Klinopiroksen meqakristalları tünd qara rəngli olub, boz rəngli tefrit tərkibli brekçiyaların içərisində qeyri-düzgün formada müşahidə olunur. Onun ana süxurunda təmas zonası nəzərə çarpır. Talış zonasında da pikritlər subqələvi seriyaya aid, xarakterik möhtəvi strukturlu olub, onların əsas kütlələri isə dolerit və subdolerit quruluşludur. Möhtəvilərin içərisində olivinlə yanaşı klinopiroksen fenokristalları iştirak edir. Həmin fenokristallar əksər hallarda iri uzunsov, bəzən lövhəvari kristallar əmələ gətirirlər. Əksər hallarda rəngsiz olurlar. Lakin onların içərisində müxtəlif ölçülü olivin və xromşpinel daxilolmaları müşahidə olunur. Klinopiroksenlərin kifayət qədər iri ölçülü prizmatik fenokristalları (1,5-2,3 sm) floqopitli, olivinli pikritlərin tərkiblərində iştirak edirlər. Bu fenokristallar olivinə nisbətən ksenomorfdur. Talış zonasınının pikritlərində isə klinopiroksenlərin tərkibi diopsid-salitə uyğun gəlir. Beləliklə, Kiçik Qafqaz və Talış zonasının pikritlərində pikroksenlərin tərkibinin dəyişməsi kristallaşma diferensiasiyası ilə tənzimlənir.

***Açar sözlər****: Kiçik Qafqaz, Talış zonası, pikrit, zonal piroksen, kristallaşma diferensiasiyası*